INTERNATIONAL JOURNAL OF ADAPTIVE CONTROL AND SIGNAL PROCESSING
Int. J. Adapt. Control Signal Process. 2016; **30**:1375–1388
Published online 18 January 2016 in Wiley Online Library (wileyonlinelibrary.com). DOI: 10.1002/acs.2659

Multi-input adaptive notch filter and observer for circadian phase estimation

Agung Julius[1,*,†], Jiaxiang Zhang[1,2], Wei Qiao[1] and John T. Wen[1]

[1]*Department of Electrical, Computer, and Systems Engineering, Rensselaer Polytechnic Institute, Troy, NY 12180, USA*
[2]*Corning Inc., Corning, NY 14831, USA*

SUMMARY

Accurate estimation of circadian phase is critical to the assessment and treatment of circadian disruption. Direct measurements of circadian rhythm markers such as dim light melatonin onset and core body temperature are inconvenient and acquired at best at low rate. On the other hand, measurements of other circadian rhythm-modulated signals such as actigraphy, heart rate, and body temperature are convenient but are typically masked by many other factors.

In this paper, we present a new multi-input adaptive notch filter algorithm that can be used to extract the periodic components from multiple circadian signals simultaneously. We also prove some stability properties of the proposed filter. Once the periodic components are extracted, the next step is to relate their phases with the circadian phase. For this, we propose a nonlinear observer, which is based on a model of the circadian phase dynamics. The model takes the form of a first-order ODE, incorporating the concept of phase response curve, which is widely used in the study of biological oscillators. We also prove the stability of the observer. We evaluate our algorithms using simulation data generated from a circadian rhythm model for fruit flies (*Drosophila melanogaster*). Copyright © 2016 John Wiley & Sons, Ltd.

Received 1 March 2015; Revised 21 September 2015; Accepted 1 December 2015

KEY WORDS: ANF; circadian rhythm; stability

1. INTRODUCTION

Circadian rhythms are biological processes found in all living organisms, from plants to insects and mammals, which repeat with a period around 24 h. The 24-h patterns of light and dark are the strongest synchronizer of circadian rhythms to the solar day. Disruption of the synchrony between the solar day and human internal master clock that regulates and generates circadian rhythms has been linked to a variety of maladies. Circadian disruption, as experienced by night-shift workers or by those traveling across multiple time zones, can lead to low productivity, digestive problems, and decreased sleep effectiveness. Long-term effects of circadian disruption has been linked to serious health problems, such as increased risk of cancer, cardiovascular disease, diabetes, and obesity.

Various groups have investigated the possibility of regulating the circadian rhythm. Light, the strongest known influence to the circadian rhythm, has been widely proposed as the control input for circadian regulation [1–8] . There are also commercial products for self-administered light therapy to address seasonal affective disorder [9, 10]. Circadian regulation using chemical intervention (e.g., melatonin and modafinil) has also been studied [11, 12].

Most of the work on light-based circadian rhythm regulation is open loop in nature, based on the phase response curve (PRC), the amount of the steady-state phase shift due to a specified light

*Correspondence to: Agung Julius, Department of Electrical, Computer Systems Engineering, Rensselaer Polytechnic Institute, Troy, NY 12180, USA.
[†]E-mail: juliua2@rpi.edu

pulse input at different circadian phases [11, 13]. Optimal control has only been recently considered [8, 14, 15]. The available commercial lighting products for circadian regulation are of low cost and convenient but only provide a rough guideline on their usage for circadian rhythm regulation. Feedback control of the light therapy is attractive as it could accommodate variations between individuals and disturbances from the environment. Some closed-loop strategies have been suggested and demonstrated in simulation [7, 16], but a reasonable estimation of the circadian phase based on physiological sensor measurements is needed for deployment.

The circadian phase may be assessed by measuring biomarkers such as the concentration of proteins that participate in the circadian rhythm regulation. For humans, certain hormones related to circadian rhythm such as melatonin, cortisol, and alpha amyloid have also been used as circadian phase markers. These types of direct measurements are intrusive in terms of collection (blood serum and saliva), time-consuming, and expensive in terms of analysis. As a result, the sampling rate is very low, at best several samples per hour, over a limited duration in experimental trials. As alternatives, the use of indirect phase markers, such as body temperature, heart/pulse rate, and activity level, is common. Locomotor activity, in particular, together with tools such as actogram (or actigraph) devices, has long been used in *Drosophila*, rodent, and human studies [17–22].

Numerous techniques for circadian phase extraction have been proposed (see review in [23]). Most rely on batch processing; that is, the circadian phase is extracted in the postprocessing of a batch of circadian data. These techniques include manual inspection of actogram [24], statistical method [25], Fourier analysis [23], cosinor [26], and activity onset [27]. A number of recursive methods, where circadian phase estimate is updated upon the availability of new data in each recursion, have also been proposed. There are two classes of algorithms, depending on whether an underlying input/output model is assumed. Extended Kalman filter [28] and particle filter [29] are model-based methods using the empirical nonlinear oscillator model (relating input light intensity to the output core body temperature). Gliding cosinor is a model-free approach that works the same as the cosinor but for a fixed window of the past data [30].

In this paper, we address two important questions related to circadian phase estimation from biometric measurement signals. First, how do we extract the periodic components from multiple biometric signals simultaneously? Second, if we are able to extract phase information from the biometric signals, how can we relate that with the circadian phase?

The first question is motivated by the increasing availability of personal fitness tracker devices that measure, for example, actigraphy, heart rate, body temperature, and perspiration. To address the first question, we present a multi-input version of the adaptive notch filter (ANF) algorithm [31, 32]. Our algorithm can extract the periodic components from the multiple signals. We also prove local stability properties of the proposed multi-input ANF algorithm and provide simulation results to assess its performance. To address the second question, we assume that the circadian phase and the biometric signal phases differ by constant phase lags. Then, we present an observer algorithm that estimates the phase lags based on the circadian phase dynamics predicted by the PRC.

2. EXTRACTION OF PERIODIC COMPONENTS FROM BIOMETRIC SIGNALS

The circadian biometric data are approximately periodic signals. Their waveforms vary with the species, individuals in the species, types of physiological measurement, and environment condition. We assume that we have a family of N circadian signals:

$$y_k(t) = a_k \sin\left(\omega^* t + \phi_k\right) + d_k,\ k \in \{1, \cdots, N\}, \tag{1}$$

where ω^* is the circadian angular frequency, ϕ_k is the phase offset of the kth signal, and d_k is its constant bias. Note that each circadian signal has different phase offsets. This represents the fact that different biometric signals (e.g., body temperature and actigraphy) peak at different times of the day. We define the phases of the different circadian signals as

DOI: 10.1002/acs

$$\theta_k(t) = \omega^* t + \phi_k,\ k \in \{1, \ldots, N\}. \tag{2}$$

Problem
Given measurements of $\{y_k(t)\}_{k=1}^N$, determine ω^* and $\{\theta_k(t)\}_{k=1}^N$.

There are several algorithms for adaptive frequency estimation [33] with relative performance trade-offs in terms of the rate of convergence, domain of convergence, robustness with respect to noise and distortion, and so on. We will focus on the ANF approach in this paper because of its stability property and superior convergence property under good initial guess of the period.

2.1. The original adaptive notch filter

The original ANF algorithm was proposed by Regalia as a discrete-time filter [34]. It was later transposed to continuous time in [31]. A realization of the filter is shown in the following.

$$\dot{x}_1 = x_2, \tag{3a}$$

$$\dot{x}_2 = -\omega^2 x_1 + (y - \hat{y}), \tag{3b}$$

$$\dot{\omega} = -\gamma x_1 (y - \hat{y}), \tag{3c}$$

$$\hat{y} = 2\zeta\omega x_2. \tag{3d}$$

The input to this filter is a sinusoidal signal

$$y(t) = a \sin\left(\omega^* t + \phi\right), \tag{4}$$

with unknown frequency ω^*. The ANF filter estimates this frequency with the state variable ω. The state variables x_1 and x_2 constitute a second-order damped oscillator that tracks the sinusoidal signal $y(t)$ with $\hat{y}(t)$. The parameters γ and ζ represent the adaptation gain and the damping factor of the oscillator, respectively. We can observe that a periodic solution of (3), which corresponds to perfect tracking $\hat{y}(t) = y(t)$, is given by

$$\bar{\omega}(t) = \omega^*, \tag{5}$$

$$\bar{x}_1(t) = \frac{-a}{2\zeta\omega^{*2}} \cos\left(\omega^* t + \phi\right), \tag{6}$$

$$\bar{x}_2(t) = \frac{a}{2\zeta\omega^*} \sin\left(\omega^* t + \phi\right). \tag{7}$$

In a later publication, Hsu *et al*. [32] proved the global convergence of a scaled version of this frequency estimator, where the input term y is scaled by ω^2. Note that this ANF can only track a single sinusoid with zero mean. An extension of the ANF idea to track signals with multiple harmonics has been reported in [35], which includes a proof of local stability.

2.2. Proposed multi-input adaptive notch filter

Note that, in principle, to handle the problem posed in Section 2, we can use a bank of N ANFs operating independently. However, we propose a solution that has the structure of interconnected N ANFs. The kth ANF tracks $y_k(t)$:

$$\dot{x}_{1,k} = x_{2,k}, \tag{8a}$$

DOI: 10.1002/acs

$$\dot{x}_{2,k} = -\omega^2 x_{1,k} + \omega^2 (y_k - \hat{y}_k), \tag{8b}$$

$$\dot{x}_{3,k} = \gamma_d (y_k - \hat{y}_k), \tag{8c}$$

$$\hat{y}_k = \frac{2\zeta x_{2,k}}{\omega} + x_{3,k}. \tag{8d}$$

The states $(x_{1,k}, x_{2,k})$ track the sinusoidal component of y_k by using the ANF algorithm of Hsu *et al*. [32]. We add another state $x_{3,k}$ that tracks the constant bias of the signal. The ANFs are interconnected through the common frequency variable ω, which is updated according to

$$\dot{\omega} = -\gamma\omega^2 \sum_{k=1}^{N} x_{1,k} \left(y_k - \hat{y}_k\right). \tag{9}$$

Under the input given in (1), the system has an equilibrium at

$$\bar{\omega} = \omega^*, \tag{10}$$

$$\bar{x}_{1,k}(t) = -\frac{a_k}{2\zeta} \cos\left(\omega^* t + \phi_k\right), \tag{11}$$

$$\bar{x}_{2,k}(t) = \dot{x}_{1,k}(t) = \frac{\omega^* a_k}{2\zeta} \sin\left(\omega^* t + \phi_k\right), \tag{12}$$

$$\bar{x}_{3,k}(t) = d_k. \tag{13}$$

Note that this equilibrium corresponds to perfect tracking by the ANFs, $\omega = \omega^*$, and $y_k = \hat{y}_k$, $k \in \{1, \cdots, N\}$. In the following section, we will prove that this equilibrium is locally stable.

3. STABILITY PROPERTIES OF THE MULTI-INPUT ADAPTIVE NOTCH FILTER

For a system consisting of N ANFs, we have a $(3N + 1)$-dimensional nonlinear system. The states of the nonlinear system can be written as

$$\left[\, x^T \;\; \omega \,\right]^T, \text{ where } x \triangleq \left[\, x_1^T \;\; \cdots \;\; x_N^T \,\right]^T$$

and

$$x_k \triangleq \left[\, x_{1,k} \;\; x_{2,k} \;\; x_{3,k} \,\right]^T.$$

We then have

$$\frac{d}{dt}\begin{bmatrix} x_1 \\ x_2 \\ \vdots \\ x_N \end{bmatrix} = \underbrace{\begin{bmatrix} A & 0 & \cdots & 0 \\ 0 & A & \cdots & 0 \\ \vdots & \vdots & \ddots & \vdots \\ 0 & 0 & \cdots & A \end{bmatrix}}_{\triangleq \mathcal{A}} \begin{bmatrix} x_1 \\ x_2 \\ \vdots \\ x_N \end{bmatrix} + \underbrace{\begin{bmatrix} B & 0 & \cdots & 0 \\ 0 & B & \cdots & 0 \\ \vdots & \vdots & \ddots & \vdots \\ 0 & 0 & \cdots & B \end{bmatrix}}_{\triangleq \mathcal{B}} Y(t), \tag{14}$$

$$\dot{\omega} = -\gamma\omega^2 \sum_{k=1}^{N} x_{1,k} \left(y_k - \frac{2\zeta}{\omega} x_{2,k} - x_{3,k}\right), \tag{15}$$

where

DOI: 10.1002/acs

$$Y(t) \triangleq \left[\, y_1(t) \;\cdots\; y_N(t) \,\right]^T,$$
$$A \triangleq \begin{bmatrix} 0 & 1 & 0 \\ -\omega^2 & -2\zeta\omega & -\omega^2 \\ 0 & -\frac{2\zeta\gamma_d}{\omega} & -\gamma_d \end{bmatrix},\; B \triangleq \begin{bmatrix} 0 \\ \omega^2 \\ \gamma_d \end{bmatrix}.$$

We can state the stability property of this multi-input ANF as follows.

Theorem 1
The multi-input ANF given by (14) and (15), under the input signal in (1), is (locally) stable at the equilibrium given by (10)–(13) for a small enough γ.

Proof
Our proof is based on the integral manifold of slow adaptation [36] , which was also used in the stability proof of the first-order ANF [32]. The idea is to consider ω as a parameter whose dynamics is much slower than the other states. This is indeed the case for the small enough γ. We denote the steady-state response of a linear time-invariant system (14), for a fixed ω under the input $Y(t)$ as $x^*(t,\omega)$. We proceed with showing that for any positive ω, γ_d, and ζ, the following are true:

(**a**) $\mathcal{A}$ is Hurwitz.
(**b**) $x^*(t,\omega)$ and $\frac{\partial}{\partial\omega}x^*(t,\omega)$ are bounded, and the latter is Lipschitz in ω.
(**c**) The right-hand side of (15) is continuous and Lipschitz in ω and y.

(Proof of **a**) Because $\mathcal{A}$ is block diagonal, it is sufficient to show that each block, that is, A, is Hurwitz. We show this by calculating the characteristic polynomial of A,

$$\chi(s) = s^3 + (2\zeta\omega + \gamma_d)\, s^2 + \omega^2 s + \gamma_d\omega^2.$$

Performing a Routh–Hurwitz test on this polynomial shows that indeed A is Hurwitz.

(Proof of **b**) $x^*(t,\omega)$ is bounded because the transfer function from $Y(t)$ to $x^*(t,\omega)$ is a block diagonal of stable rational transfer functions. Each of the block is given by

$$H(s) \triangleq (sI - A)^{-1}B = \begin{bmatrix} \frac{\omega^2 s}{s^3+(2\zeta\omega+\gamma_d)s^2+\omega^2 s+\gamma_d\omega^2} \\ \frac{\omega^2 s^2}{s^3+(2\zeta\omega+\gamma_d)s^2+\omega^2 s+\gamma_d\omega^2} \\ \frac{\gamma_d s^2+\gamma_d\omega^2}{s^3+(2\zeta\omega+\gamma_d)s^2+\omega^2 s+\gamma_d\omega^2} \end{bmatrix}. \tag{16}$$

Observing that

$$H(j\omega^*) = \begin{bmatrix} \frac{j\omega^2\omega^*}{j\omega^*(\omega^2-\omega^{*2})+\gamma_d(\omega^2-\omega^{*2})-2\zeta\omega\omega^{*2}} \\ \frac{-\omega^2\omega^{*2}}{j\omega^*(\omega^2-\omega^{*2})+\gamma_d(\omega^2-\omega^{*2})-2\zeta\omega\omega^{*2}} \\ \frac{\gamma_d(\omega^2-\omega^{*2})}{j\omega^*(\omega^2-\omega^{*2})+\gamma_d(\omega^2-\omega^{*2})-2\zeta\omega\omega^{*2}} \end{bmatrix} \tag{17}$$

and that the coefficients of the transfer functions are all polynomials in ω, $\frac{\partial}{\partial\omega}x^*(t,\omega)$ is bounded and Lipschitz in ω. Point (**c**) is straightforward from (15).

Using the preceding facts (a–c) and Theorems 3.1 and 5.1 from [36], we can infer the following:

(1) The existence of an integral manifold M_γ for a small enough γ. For a $\gamma > 0$, the integral manifold $M_\gamma \subset \mathbb{R}^{3N+1}$ is a time-varying one-dimensional surface such that

$$(x(t_0), \omega(t_0)) \in M_\gamma \Rightarrow (x(t), \omega(t)) \in M_\gamma,$$

for all $t \geqslant t_0$. Note that, at the manifold, M_γ contains the equilibrium given by (10)–(13). Further, as $\gamma \to 0$, M_γ arbitrarily approaches M_0.
(2) The integral manifold M_γ is locally attractive.

DOI: 10.1002/acs

To show that the ω adaptation dynamics is stable, we follow the same reasoning as in [32, 35]. First, notice that if $\gamma \ll 1$, the dynamics of ω is very slow, and thus, we can approximate (15) with

$$\dot{\omega} = -\gamma\omega^2 \sum_{k=1}^{N} x_{1,k}^* \left(y_k - \frac{2\zeta}{\omega} x_{2,k}^* - x_{3,k}^* \right). \tag{18}$$

Now, we again use the fact that the oscillation of x^* is much faster than the dynamics of ω and define the averaged system

$$\dot{\omega}_{\text{av}} = -\gamma\omega_{\text{av}}^2 \left[\sum_{k=1}^{N} x_{1,k}^* \left(y_k - \frac{2\zeta}{\omega_{\text{av}}} x_{2,k}^* - x_{3,k}^* \right) \right]_{\text{av}}, \tag{19}$$

$$= -\gamma\omega_{\text{av}}^2 \sum_{k=1}^{N} \left(\left[x_{1,k}^* y_k \right]_{\text{av}} - \frac{2\zeta}{\omega_{\text{av}}} \left[x_{1,k}^* x_{2,k}^* \right]_{\text{av}} - \left[x_{1,k}^* x_{3,k}^* \right]_{\text{av}} \right), \tag{20}$$

where the operation $[x(t)]_{\text{av}}$ denotes averaging

$$[x(t)]_{\text{av}} \triangleq \frac{1}{T} \int_0^T x(t)\, dt = \frac{\omega^*}{2\pi} \int_0^T x(t)\, dt. \tag{21}$$

Using Lemma 2, we can establish

$$\dot{\omega}_{\text{av}} = -\gamma\omega_{\text{av}}^2 \sum_{k=1}^{N} \frac{\omega_{\text{av}}^2 \omega^{*2} \left(\omega_{\text{av}}^2 - \omega^{*2} \right) a_k^2}{\left(\gamma_d \left(\omega_{\text{av}}^2 - \omega^{*2} \right) - 2\zeta\omega_{\text{av}}\omega^{*2} \right)^2 + \omega^{*2} \left(\omega_{\text{av}}^2 - \omega^{*2} \right)^2}. \tag{22}$$

Observe that the dynamics in (22) has an equilibrium at $\omega_{\text{av}} = \omega^*$. Further, by linearizing the dynamics about this equilibrium, we can observe that it is (locally) stable. □

Lemma 2
The following relations are true:

$$\begin{aligned} \left[x_{1,k}^* y_k \right]_{\text{av}} &= \frac{\omega^2 \omega^{*2} \left(\omega^2 - \omega^{*2} \right) a_k^2}{\left(\gamma_d \left(\omega^2 - \omega^{*2} \right) - 2\zeta\omega\omega^{*2} \right)^2 + \omega^{*2} \left(\omega^2 - \omega^{*2} \right)^2}, \\ \left[x_{1,k}^* x_{2,k}^* \right]_{\text{av}} &= 0, \\ \left[x_{1,k}^* x_{3,k}^* \right]_{\text{av}} &= 0. \end{aligned}$$

Proof
Let us define the shorthand notation

$$A\angle\theta \triangleq A \sin\left(\omega^* t + \theta \right).$$

Hence, from (1), we have

$$y_k = d_k + a_k \angle\theta_k. \tag{23}$$

From (17), we then have

DOI: 10.1002/acs

$$x^*_{1,k} = \frac{\omega^2\omega^* a_k}{\sqrt{\left(\gamma_d\left(\omega^2-\omega^{*2}\right)-2\zeta\omega\omega^{*2}\right)^2+\omega^{*2}\left(\omega^2-\omega^{*2}\right)^2}}$$
$$\angle\left(\theta_k+\frac{\pi}{2}-\tan^{-1}\frac{\omega^*\left(\omega^2-\omega^{*2}\right)}{\gamma_d\left(\omega^2-\omega^{*2}\right)-2\zeta\omega\omega^{*2}}\right),$$
$$x^*_{2,k} = \frac{\omega^2\omega^{*2} a_k}{\sqrt{\left(\gamma_d\left(\omega^2-\omega^{*2}\right)-2\zeta\omega\omega^{*2}\right)^2+\omega^{*2}\left(\omega^2-\omega^{*2}\right)^2}}$$
$$\angle\left(\theta_k+\pi-\tan^{-1}\frac{\omega^*\left(\omega^2-\omega^{*2}\right)}{\gamma_d\left(\omega^2-\omega^{*2}\right)-2\zeta\omega\omega^{*2}}\right).$$

Also, if $\omega > \omega^*$,

$$x^*_{3,k} = d_k + \frac{\gamma_d\left(\omega^2-\omega^{*2}\right)a_k}{\sqrt{\left(\gamma_d\left(\omega^2-\omega^{*2}\right)-2\zeta\omega\omega^{*2}\right)^2+\omega^{*2}\left(\omega^2-\omega^{*2}\right)^2}}$$
$$\angle\left(\theta_k-\tan^{-1}\frac{\omega^*\left(\omega^2-\omega^{*2}\right)}{\gamma_d\left(\omega^2-\omega^{*2}\right)-2\zeta\omega\omega^{*2}}\right),$$

and if $\omega < \omega^*$,

$$x^*_{3,k} = d_k + \frac{-\gamma_d\left(\omega^2-\omega^{*2}\right)a_k}{\sqrt{\left(\gamma_d\left(\omega^2-\omega^{*2}\right)-2\zeta\omega\omega^{*2}\right)^2+\omega^{*2}\left(\omega^2-\omega^{*2}\right)^2}}$$
$$\angle\left(\theta_k+\pi-\tan^{-1}\frac{\omega^*\left(\omega^2-\omega^{*2}\right)}{\gamma_d\left(\omega^2-\omega^{*2}\right)-2\zeta\omega\omega^{*2}}\right).$$

We also have that

$$[A_1\angle\theta_1 \cdot A_2\angle\theta_2]_{\text{av}} = \frac{A_1A_2}{2}\cos(\theta_1-\theta_2). \tag{24}$$

It follows immediately that $[x^*_{1,k}x^*_{2,k}]_{\text{av}} = 0$ and $[x^*_{1,k}x^*_{3,k}]_{\text{av}} = 0$ because the phase difference between the two components is $\frac{\pi}{2}$. Further,

$$\left[x^*_{1,k}y_k\right]_{\text{av}} = \frac{\omega^2\omega^* a_k^2}{\sqrt{\left(\gamma_d\left(\omega^2-\omega^{*2}\right)-2\zeta\omega\omega^{*2}\right)^2+\omega^{*2}\left(\omega^2-\omega^{*2}\right)^2}}$$
$$\sin\left(\tan^{-1}\frac{\omega^*\left(\omega^2-\omega^{*2}\right)}{\gamma_d\left(\omega^2-\omega^{*2}\right)-2\zeta\omega\omega^{*2}}\right), \tag{25}$$
$$= \frac{\omega^2\omega^{*2}\left(\omega^2-\omega^{*2}\right)a_k^2}{\left(\gamma_d\left(\omega^2-\omega^{*2}\right)-2\zeta\omega\omega^{*2}\right)^2+\omega^{*2}\left(\omega^2-\omega^{*2}\right)^2}.$$

□

We simulate the application of the proposed multi-input ANF, as shown in Figure 1. For this simulation, we use the parameter values $\gamma = 0.02$, $\gamma_d = 1$, and $\zeta = 0.5$. To evaluate the ability of the filter to handle (slowly) varying frequency, we simulate input signals whose frequency periodically switches between $\omega^* = 10$ rad/s and $\omega^* = 20$ rad/s, as shown in Figure 2. Finally, we artificially add (uncorrelated) white noise signals to each of the inputs. The results from the proposed multi-input ANF algorithm are shown in Figure 3.

DOI: 10.1002/acs

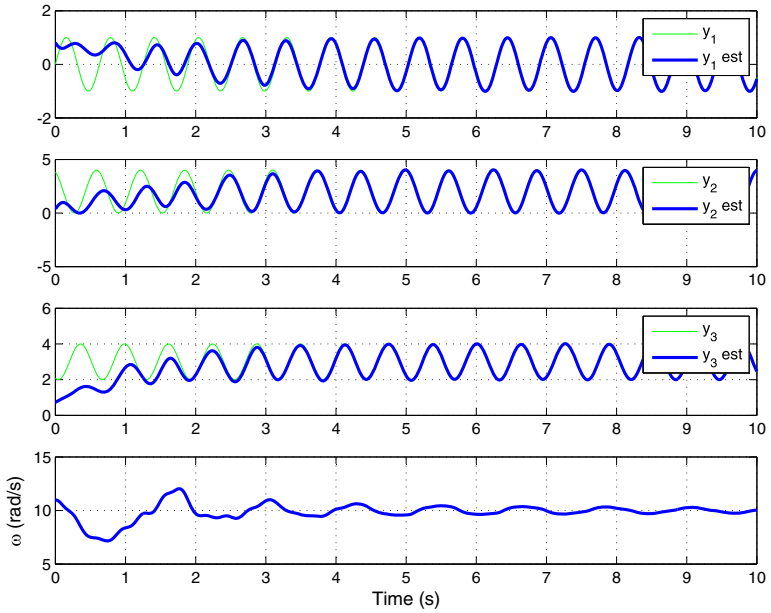

Figure 1. A simulation of the multi-input adaptive notch filter (ANF) with three inputs. The top three panels show that outputs of the ANF ($\hat{y}_{1,2,3}(t)$) converge to the respective inputs ($y_{1,2,3}(t)$). Note that all inputs have the same frequency ($\omega^* = 10$ rad/s), but different phases and direct-current components. The bottom panel shows the frequency estimate $\omega(t)$ converging to ω^*.

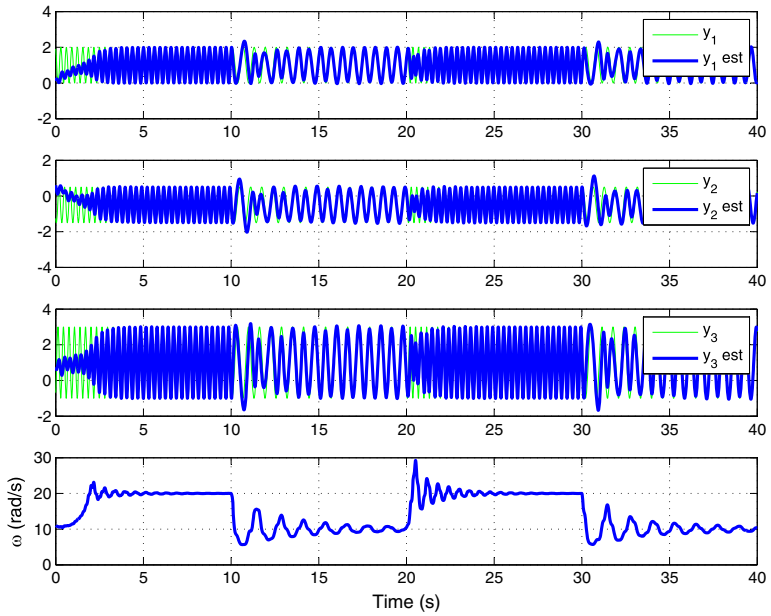

Figure 2. Simulation of the same algorithm as shown in Figure 1, using input signals with time-varying frequency.

3.1. Weighted multi-input adaptive notch filter

In general, the multi-input ANF structure allows us to assign different weights to the contribution of each ANF subsystem to the ω dynamics. This is carried out by replacing (15) with the following:

$$\dot{\omega} = -\gamma\omega^2 \sum_{k=1}^{N} W_k \; x_{1,k} \left(y_k - \frac{2\zeta}{\omega} x_{2,k} - x_{3,k} \right), \tag{26}$$

DOI: 10.1002/acs

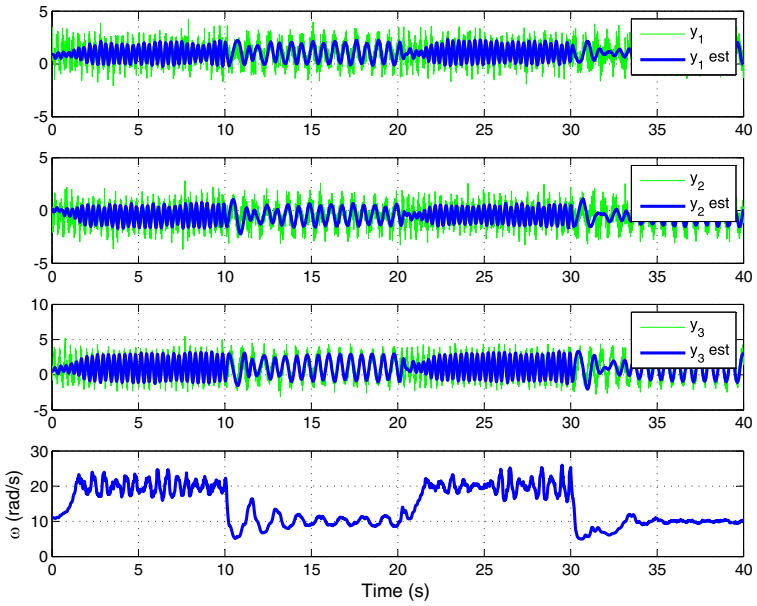

Figure 3. Simulation of the same algorithm as shown in Figure 2, using noisy input signals with time-varying frequency.

where $\{W_k\}_{k=1}^N$ are the positive weights assigned to each of the N ANF subsystems. The stability of this system can be stated as follows.

Lemma 3
The multi-input ANF given by (14) and (26), under the input signal in (1), is (locally) stable at the equilibrium given by (10)–(13) for a small enough γ.

Proof
The proof follows that of Theorem 1 up to (18). In this case, we replace this equation with

$$\dot{\omega} = -\gamma\omega^2 \sum_{k=1}^{N} W_k \; x_{1,k}^* \left(y_k - \frac{2\zeta}{\omega} x_{2,k}^* - x_{3,k}^* \right), \tag{27}$$

and the averaged dynamics is given by

$$\dot{\omega}_{\text{av}} = -\gamma\omega_{\text{av}}^2 \sum_{k=1}^{N} \frac{\omega_{\text{av}}^2 \omega^{*2} \left(\omega_{\text{av}}^2 - \omega^{*2}\right) a_k^2 W_k}{\left(\gamma_d \left(\omega_{\text{av}}^2 - \omega^{*2}\right) - 2\zeta\omega_{\text{av}}\omega^{*2}\right)^2 + \omega^{*2} \left(\omega_{\text{av}}^2 - \omega^{*2}\right)^2}, \tag{28}$$

which is still locally stable at $\omega_{\text{av}} = \omega^*$. □

Note that the same reasoning for the stability property still holds if we let the weights $\{W_k\}_{k=1}^N$ be slowly time varying. Adjusting the relative weights of the different input channels can be beneficial, for example, in situations where some of the channels are (temporarily) not reliable because of high-intensity measurement noise. To simulate this situation, we modify the simulation discussed in the previous section. We inject artificial noise to one of the channels (channel 3), while the other two channels are noise free. We run two simulations. In the first one, all channels are given equal weights. In the second simulation, channel 3 is given zero weight, while the weights of the other two channels are increased by 50%. Outputs from the two simulations can be seen in Figure 4. We measure how well the multi-input ANF algorithm tracks the signal frequency by calculating the integral square error from the two simulations. The results are shown in the same figure. We can see, as expected, that decoupling the noisy channel improves the performance of the filter.

DOI: 10.1002/acs

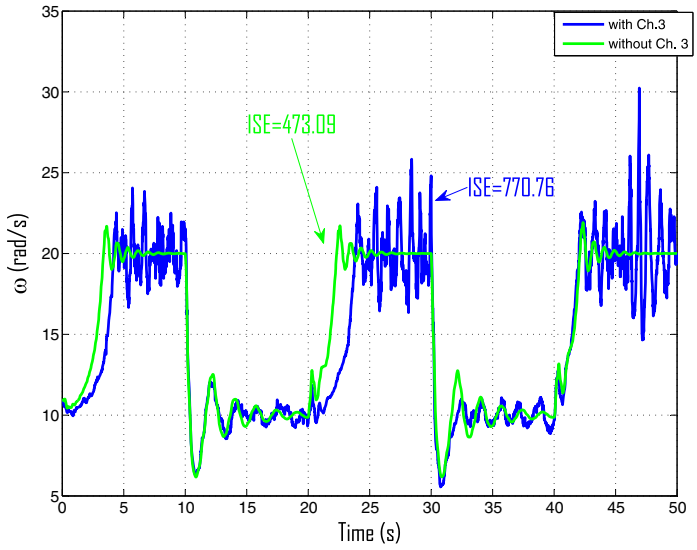

Figure 4. Comparing the performance of the adaptive notch filter with and without a noisy input channel. The performance measure is the integral square error (ISE) of ω versus ω^*.

4. ESTIMATION OF CIRCADIAN PHASE

In the previous sections, we presented an algorithm for extracting the periodic components from multiple possibly noisy circadian signals simultaneously. Assuming that this is done, the next question to address is how to determine the circadian phase from the circadian signal phases. We formulate the problem as follows. Suppose that the circadian phase dynamics is given by

$$\dot{\theta} = \omega_0 + f(\theta)u, \tag{29}$$

where ω_0 is the so-called free-running frequency (nominally around $2\pi/24$ rad/h) and $f(\theta)$ is the phase response function, which is assumed to be known. The input u is the incoming circadian light stimuli to the subject, which is assumed to be measured. Therefore, $f(\theta)$ describes how the light input affects the dynamics of the circadian phase, and ω_0 describes the oscillation frequency in the absence of light input ($u(t) \equiv 0$).

The circadian phase θ is the variable that we want to estimate. We assume that, in addition to the light input $u(t)$, we also have the measurements of the circadian signal phases (2)

$$\theta_k(t) = \theta(t) - \Delta_k,\ k \in \{1, \cdots, N\}. \tag{30}$$

The phase lags $\{\Delta_i\}_{i=1}^N$ are constant but unknown.

Problem
Given measurements of $u(t)$ and $\{\theta_k(t)\}_{k=1}^N$, determine $\{\Delta_i\}_{i=1}^N$ and $\theta(t)$.

We approach this problem by using a nonlinear observer detailed in the following. First, we assume the following is true about our system:

(A1) The light input and the phase dynamics are such that

$$\int_0^\infty \left(\frac{df}{d\theta}\bigg|_{\theta=\theta(t)} \right)^2 u(t)\, dt = \infty.$$

Essentially, this assumption means that the light input affects the phase dynamics in a significant way persistently. In practice, this assumption is mild and is typically true. Most PRCs are not flat, and for a typical natural periodic light–dark pattern,

DOI: 10.1002/acs

$$\int_{\text{period}} \left(\frac{df}{d\theta}\bigg|_{\theta=\theta(t)} \right)^2 u(t)\, dt > 0. \tag{31}$$

Under the preceding assumption, we propose the following nonlinear observer:

$$\frac{d}{dt}\hat{\Delta}_k = L_k \cdot \frac{df}{d\theta}\bigg|_{\theta=\theta_k+\hat{\Delta}_k} \left(\dot{\theta}_k - \omega_0 - f(\theta_k + \hat{\Delta}_k)u(t) \right),\ k \in \{1, \cdots, N\}, \tag{32}$$

where $\hat{\Delta}_k$ is the estimated Δ_k. The term $\{L_k\}_{k=1}^N$ is the positive observer gains.

We can rewrite the dynamics of $e_k \triangleq \hat{\Delta}_k - \Delta_k$ as

$$\frac{d}{dt}e_k = L_k \frac{df}{d\theta}\bigg|_{\theta=\theta_k+\Delta_k+e_k} \left(f(\theta_k + \Delta_k) - f(\theta_k + \Delta_k + e_k) \right) u(t). \tag{33}$$

Lemma 4

The time-varying dynamics in (33) is locally exponentially stable at $e_k = 0$.

Proof

First of all, we observe that $e_k = 0$ is an equilibrium of (33). Next, we linearize the right-hand side around the equilibrium and obtain

$$\frac{d}{dt}e_k \approx -L_k \left(\frac{df}{d\theta}\bigg|_{\theta=\theta(t)} \right)^2 u(t) \cdot e_k. \tag{34}$$

Based on Assumption A1, the linearized dynamics is exponentially stable, and hence, by Theorem 4.13 in [37], this lemma is proven. □

5. APPLICATION ON SIMULATED CIRCADIAN SIGNALS

We simulate a widely used model for circadian rhythm in fruit flies (*Drosophila melanogaster*) published by Leloup and Goldbeter [38]. The model is a system of nonlinear ODEs with 10 states that

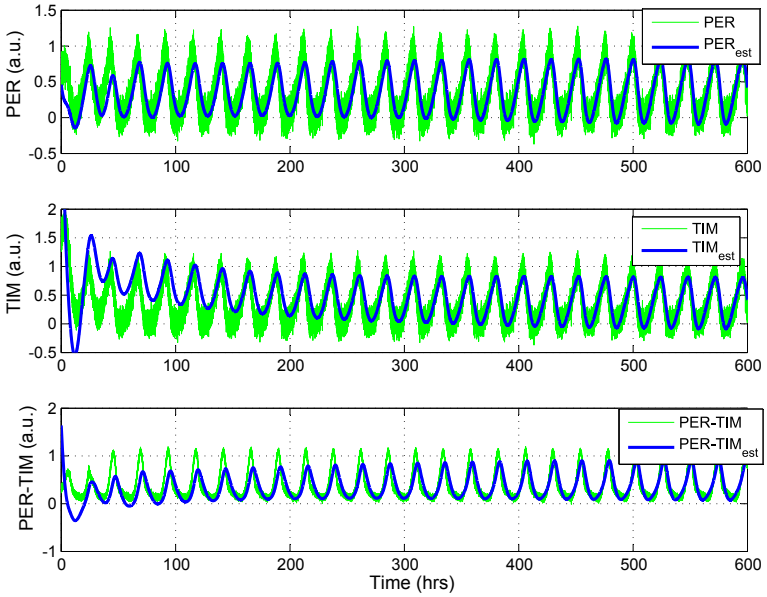

Figure 5. Applying the multi-input adaptive notch (ANF) filter algorithm on simulated circadian signals from the *Drosophila* circadian model. We simulate the concentrations of the proteins period (PER), timeless (TIM), and PER–TIM with arbitrary units (a.u.). PER_{est}, TIM_{est}, and $\text{PER–TIM}_{\text{est}}$ are the outputs of the ANF.

DOI: 10.1002/acs

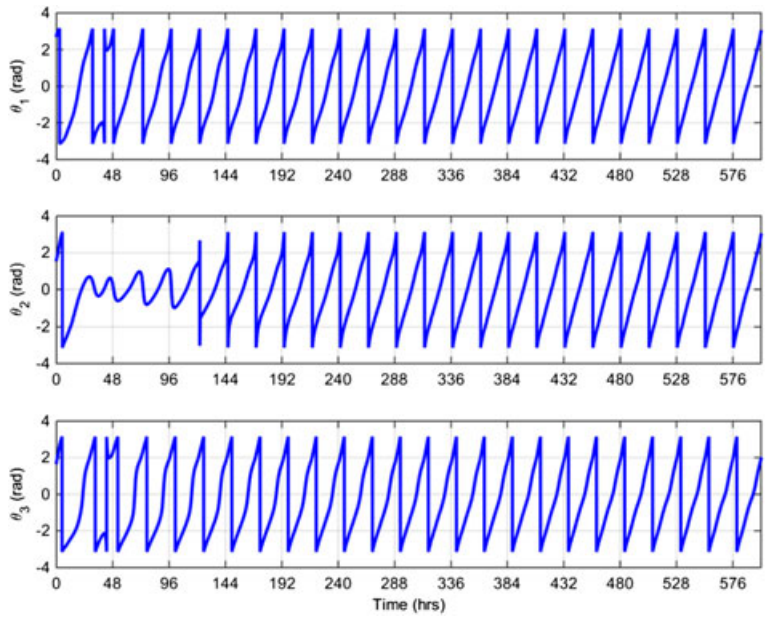

Figure 6. Estimation of the phases of the circadian signals shown in Figure 5.

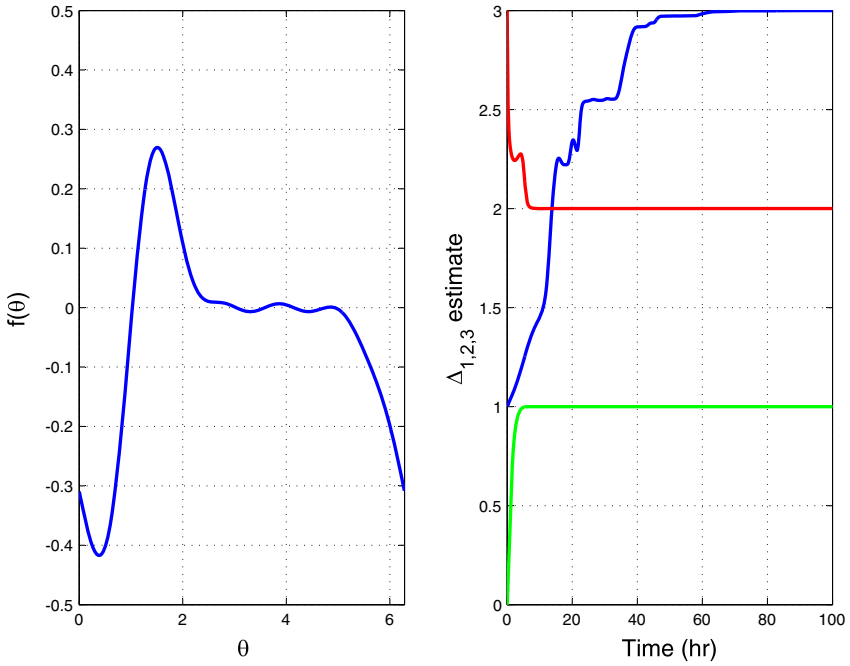

Figure 7. (left) The phase response of *Drosophila* $f(\theta)$. (right) The evolution of $\hat{\Delta}_k$ for $k = 1, 2, 3$. The actual Δ_k are 1, 2, and 3.

capture the circadian oscillations of the period (PER) and timeless (TIM) proteins in *Drosophila*. The oscillation happens because the expressions of both the PER and TIM proteins are repressed by the PER–TIM protein complex. The oscillation is essentially a product of a nonlinear negative feedback in circadian gene expression regulation.

In our simulation, we assume that we can measure the concentration of the PER, TIM, and PER–TIM proteins. We use these three signals as the inputs to our multi-input ANF. The simulation results, obtained with parameter values $\zeta = 0.5$, $\gamma = 0.06$, and $\gamma_d = 0.01$, are shown in Figure 5.

DOI: 10.1002/acs

In Figure 6, we can also see the estimation of the phases of the circadian signals. Based on (8), the phase of the kth ANF is defined by

$$\hat{\theta}_k(t) \triangleq \tan^{-1} \frac{x_{2,k}(t)}{-\omega \cdot x_{1,k}(t)}. \tag{35}$$

Next, we apply our nonlinear observer algorithm on the phase dynamics of the *Drosophila* circadian model. The phase response function $f(\theta)$ of this model is shown in Figure 7 (left). The angular velocity is $\omega_0 = \frac{2\pi}{24}$ rad/h. We simulate the dynamics given by (29) and (30) for $\Delta_{1,2,3} = 1, 2, 3$. We choose $L_{1,2,3} = 10$ for the gains in the observer dynamics given in (32). The estimate $\hat{\Delta}_{1,2,3}$ can be seen in Figure 7 (right) to converge to the actual values.

6. CONCLUSIONS AND DISCUSSION

Motivated by the necessity for estimating the circadian phase in closed-loop circadian rhythm control, we present two algorithms in this paper. The first algorithm is a generalization of the ANF algorithm, with which we can simultaneously extract the periodic components of multiple circadian signals. The second algorithm is essentially a nonlinear observer for estimating the circadian phase from the phases of the circadian signals. We also prove some stability properties for both algorithms.

With the proliferation of personal devices capable of collecting biometric data that can be used as circadian signals, such as actigraphy, heart rate, and body temperature, the algorithms presented here can enable personalized circadian rhythm estimation and control. Therefore, efficient implementation of these algorithms on mobile computing devices and further theoretical generalizations such as multi-input multi-harmonics ANF are interesting future research directions.

ACKNOWLEDGEMENTS

This work was supported by the National Science Foundation (NSF) Smart Lighting Engineering Research Center (EEC-0812056), Army Research Office grant W911NF-11-1-0490, and in part by the Center for Automation Technologies and Systems (CATS) under a block grant from the New York State Empire State Development Division of Science, Technology and Innovation (NYSTAR) contract C090145. The authors would also like to thank Dr. Mark Rea, Dr. Mariana Figueiro, and Andrew Bierman at the RPI Light Research Center for introducing this topic to the authors.

REFERENCES

1. Jewett M, Kronauer R, Czeisler C. Phase-amplitude resetting of the human circadian pacemaker via bright light: a further analysis. *Journal of Biological Rhythms* 1994; **9**:295–314.
2. Jewett M, Rimmer D, Duffy J, Klerman E, Kronauer R, Czeisler C. Human circadian pacemaker is sensitive to light throughout subjective day without evidence of transients. *American Journal of Physiology—Regulatory, Integrative and Comparative Physiology* 1997; **273**:1800–1809.
3. Mott C, Mollicone D, Van Wollen M, Huzmezan M. Modifying the human circadian pacemaker using model based predictive control. *2003 American Control Conference*, Denver, CO, 2003; 453–458.
4. Bagheri N, Stelling J, Doyle III F. Optimal phase-tracking of the nonlinear circadian oscillator. *2005 American Control Conference*, Portland, OR, 2005; 3235–3240.
5. Gronfier C, Wright KP, Kronauer R, Czeisler C. Entrainment of the human circadian pacemaker to longer-than-24-h days. *Proceedings of National Academy of Science* 2007; **104**(21):9081–9086.
6. II DD, Forger D, Klerman E. Taking the lag out of jet lag through model based schedule design. *PLoS Computational Biology* June 2009; **5**(6).
7. Zhang J, Bierman A, Wen J, Julius A, Figueiro M. Circadian system modeling and phase control. *Conference on Decision and Control*, Atlanta, GA, 2010; 6058–6063.
8. Zhang J, Wen J, Julius A. Optimal circadian rhythm control with light input for rapid entrainment and improved vigilance. *Conference on decision and control*, Maui, HI, 2012; 3007–3012.
9. Philips. Product manual of HF3332 and HF3331. (Available from: http://www.lighttherapy.philips.com) [Accessed on 4 January 2016].
10. Terman M, Terman J. Light therapy for seasonal and nonseasonal depression: efficacy, protocol, safety and side effects. *CNS Spectrum* 2005; **10**(8):647.
11. Lewy A, Ahmed S, Jackson J, Sack R. Melatonin shifts human orcadian rhythms according to a phase-response curve. *Chronobiology International* 1992; **9**(5):380–392.

DOI: 10.1002/acs

12. Harrington M. Location, location, location: important for jet-lagged circadian loops. *Journal of Clinical Investigation* July 2010; **120**(7):2265–2267.
13. Minors D, Waterhouse J, Wirz-Justice A. A human phase-response curve to light. *Neuroscience Letters* 1991; **133**(1):36–40.
14. Maria ED, Fages F, Soliman S. On coupling models using model-checking: effects of irinotecan injections on the mammalian cell cycle. *CMSB'09: Seventh International Conference on Computational Methods in Systems Biology*, 2009; 142–157.
15. Maria ED, Fages F, Rizk A, Soliman S. *Design, optimization and predictions of a coupled model of the cell cycle, circadian clock, dna repair system, irinotecan metabolism and exposure control under temporal logic constraints*. pre-print submitted to Theoretical Computer Science, 2011.
16. Bagheri N, Stelling J, III FD. Circadian phase entrainment via nonlinear model predictive control. *International Journal of Robust and Nonlinear Control* 2007; **17**:1555–1571.
17. Frank K, Zimmerman W. Action spectra for phase shifts of a circadian rhythm in *Drosophila*. *Science* 1969; **163**(3868):688–689.
18. Daan S, Pittendrigh C. A functional analysis of circadian pacemakers in nocturnal rodents. II. The variability of phase response curves. *Journal on Computational Physiology* 1976; **106**:253–266.
19. Brainard G, Hanifin J, Greeson J, Byrne B, Glickman G, Gerner E, Rollag M. Action spectrum for melatonin regulation in humans: evidence for a novel circadian photoreceptor. *Journal of Neuroscience* 2001; **21**(16): 6405–6412.
20. Klarsfeld A, Leloup J, Rouyer F. Circadian rhythms of locomotor activity in drosophila. *Behavioural Processes* 2003; **64**:161–175.
21. Ancoli-Israel S, Cole R, Alessi C, Chambers M, Moorcroft W, Pollak C. The role of actigraphy in the study of sleep and circadian rhythms. American Academy of Sleep Medicine review paper. *Sleep* 2003; **26**(3):342–92.
22. Zhang J, Wen J, Julius A, Bierman A, Figueiro M. Modeling of *Drosophila* circadian system based on the locomotor activity. *2011 American Control Conference*, San Francisco, CA, June 2011; 3496–3501.
23. Refinetti R, Cornelissen G, Halberg F. Procedures for numerical analysis of circadian rhythms. *Biological Rhythm Research* 2007; **38**:275–325.
24. Refinetti R. *Circadian Physiology*. CRC Press: Boca Raton, FL, 2006.
25. Enright JT. The search for rhythmicity in biological time series. *Journal of Theoretical Biology* 1965; **8**:426–468.
26. Teicher MH, Barber NI. Cosifit: an interactive program for simultaneous multioscillator cosinor analysis of time-series data. *Computers and Biomedical Research* 1990; **23**:283–295.
27. Batschelet E. *Circular Statistics in Biology.* Academic Press.: New York, NY, 1981.
28. Indic P, Brown E. Characterizing the amplitude dynamics of the human core-temperature circadian rhythm using a stochastic–dynamic model. *Journal of Theoretical Biology* 2006; **239**(4):499–506.
29. Mott C, Dumont G, Boivin DB, Mollicone D. Model-based human circadian phase estimation using a particle filter. *IEEE Transactions on Biomedical Engineering* 2011; **58**(5):1325–1336.
30. Nintcheu-Fata S, Cornlissen G, Katinas G, Halberg F, Fier B, Siegelov J, Maek M, Duek J. Software for contour maps of moving least-squares spectra. *Scripta medica* 2003; **76**:279–283.
31. Bodson M, Douglas SC. Adaptive algorithms for the rejection of sinusoidal disturbances with unknown frequency. *Automatica* 1997; **33**(12):2213–2221.
32. Hsu L, Ortega R, Damm G. A globally convergent frequency estimator. *IEEE Transaction on Automatic Control* 1999; **44**(4):698–713.
33. Tichavsky P, Nehorai A. Comparative study of four adaptive frequency trackers. *IEEE Transaction on Signal Processing* 1997; **45**(6):1473–1484.
34. Regalia P. *IIR Filtering in Signal Processing and Control*. Marcel Dekker: New York, NY, 1995.
35. Mojiri M, Karimi-Ghartemani M, Bakshai A. Time-domain signal analysis using adaptive notch filter. *IEEE Transactions on Signal Processing* 2007; **55**(1):85–93.
36. Riedle B, Kokotovic P. Integral manifolds of slow adaptation. *IEEE Transactions on Automatic Control* 1986; **31**(4):316–324.
37. Khalil H. *Nonlinear Systems* (third). Prentice-Hall: Upper Saddle River, NJ, 2002.
38. Leloup JC, Goldbeter A. A model for circadian rhythms in *Drosophila* incorporating the formation of a complex between the PER and TIM proteins. *Journal of Biological Rhythms* 1998; **13**:70–87.

DOI: 10.1002/acs